Relativistic Hartree theory for nuclei far from the stability line

D. Hirata,[1,2] H. Toki,[1,3] T. Watabe,[3] I. Tanihata,[1] and B. V. Carlson[2]
[1]*The Institute of Physical and Chemical Research (RIKEN), Hirosawa, Wako, Saitama 351-01, Japan*
[2]*Instituto de Estudos Avançados–Centro Técnico Aeroespacial, São José dos Campos, São Paulo, Brazil*
[3]*Department of Physics, Tokyo Metropolitan University, Hachiohji, Tokyo 192, Japan*
(Received 23 January 1991)

We study nuclei far from the stability line using the relativistic Hartree theory. We calculate the properties of various elements of the Periodic Table up to the proton and neutron drip lines with several parameter sets. After comparing the numerical results, we discuss nuclear properties near the drip lines in detail for the parameter sets that include nonlinear terms in the sigma-meson Lagrangian.

I. INTRODUCTION

The recent experimental program using radioactive nuclear beams has opened for study the properties of nuclei far from the stability line [1]. In addition to the masses, nuclear radii, various moments, and the excitation spectra can be measured [2]. The use of inverse kinematics, in which light nuclear targets are bombarded with high-energy heavy ions, should provide information of the density distributions and other quantities such as the spin-orbit potential [3].

What new phenomena might be expected? All nuclei near the stability line have similar saturation densities. For nuclei far from the line, the central density could change with the neutron number (N) while the proton number (Z) remains fixed. Or the densities could remain almost constant with the proton and the neutron radii becoming very different from each other. One of the exciting findings in this respect was the neutron halo around the ^{9}Li core in ^{11}Li [2]. The two neutrons are distributed far from the ^{9}Li core. The magic numbers could also be different for nuclei far from the stability line, since they are a result of the interplay between the central potential and the spin-orbit interaction.

The study of nuclei far from the stability line will have a large impact on astrophysics. The heavy elements are produced by the s and r processes. The r process produces nuclei far from the stability line through neutron capture. While the s process site is believed to be the asymptotic giant branch in heavy stars, the r process site is still under debate [4]. It could have occurred during the big bang due to nonuniformities in the early Universe [5]. It is also possible that it takes place in supernova explosions [6]. The equation of state of neutron-rich matter is also much needed for the study of neutron stars and of supernova explosions.

One of the successful theories in describing the properties of nuclei is the relativistic Hartree theory proposed by Walecka [7]. In addition to the earlier studies [8–11], the recent extensive study by Gambhir *et al.* [12] demonstrated the good description of nuclear properties of stable nuclei obtained in the relativistic Hartree theory. Hence, the parameter sets fixed by the properties of stable nuclei seem a good starting point for calculating the properties of nuclei up to the proton and neutron drip lines. A first step in this direction was reported by Toki *et al.* [13]. However, we have to be careful to remember that the relativistic Hartree theory is an effective theory. The parameters of the coupling constants and the masses could be functions of the proton and neutron numbers. In the future, we intend to adjust the parameter sets by performing more refined calculations using the relativistic Brueckner-Hartree-Fock (RBHF) [14] or the finite nucleus G-matrix theory [15] for various proton and neutron numbers. We are also prepared to refine the calculations with new experimental results.

We arrange this paper as follows. Section II summarizes the relativistic Hartree theory used for numerical calculations. We also discuss how the various parameter sets are obtained. The numerical results are presented in Sec. III, where we compare the results obtained with the different sets. The case of a nonlinear potential for the sigma meson (NL1 and NL2) is discussed extensively. Section IV is devoted to the conclusions.

II. RELATIVISTIC HARTREE THEORY

We follow exactly the work of Walecka for the description of the relativistic Hartree theory [7]. For completeness, we write the formulae necessary for numerical calculations, which are well described in the work of Gambhir *et al.* [12]. The Lagrangian density is

$$\begin{aligned} L=&\bar{\psi}[i\gamma^{\mu}\partial_{\mu}-M]\psi+\tfrac{1}{2}\partial_{\mu}\sigma\partial^{\mu}\sigma-U(\sigma)-g_{\sigma}\bar{\psi}\psi\sigma \\ &-\tfrac{1}{4}H_{\mu\nu}H^{\mu\nu}+\tfrac{1}{2}m_{\omega}^{2}\omega_{\mu}\omega^{\mu}-g_{\omega}\bar{\psi}\gamma_{\mu}\psi\omega^{\mu} \\ &-\tfrac{1}{4}G^{a}_{\mu\nu}G^{a\mu\nu}+\tfrac{1}{2}m_{\rho}^{2}\rho^{a}_{\mu}\rho^{a\mu}-g_{\rho}\bar{\psi}\gamma_{\mu}\tau^{a}\psi\rho^{\mu a} \\ &-\tfrac{1}{4}F_{\mu\nu}F^{\mu\nu}-e\bar{\psi}\gamma_{\mu}\frac{(1-\tau_3)}{2}\psi A^{\mu}\,, \end{aligned} \tag{1}$$

where ψ is an SU(2) baryon field of mass M (protons and neutrons) and σ, ω_{μ}, and ρ^{a}_{μ} are the sigma, omega, and rho meson fields with masses m_{σ}, m_{ω}, and m_{ρ}, respectively. A_{μ} is the photon field, which generates the Coulomb interaction among protons with $e^2/4\pi=1/137$. The field tensors for the vector fields are given by

$$H_{\mu\nu}=\partial_\mu\omega_\nu-\partial_\nu\omega_\mu ,$$
$$G^a_{\mu\nu}=\partial_\mu\rho^a_\nu-\partial_\nu\rho^a_\mu-g_\rho\varepsilon^{abc}\rho^b_\mu\rho^c_\nu , \quad (2)$$
$$F_{\mu\nu}=\partial_\mu A_\nu-\partial_\nu A_\mu .$$

g_σ, g_ω, and g_ρ are the σNN, ωNN, and ρNN coupling constants. $U(\sigma)$ denotes the nonlinear potential for σ,

$$U(\sigma)=\tfrac{1}{2}m_\sigma^2\sigma^2+\tfrac{1}{3}g_3\sigma^3+\tfrac{1}{4}g_4\sigma^4 . \quad (3)$$

The Euler-Lagrange equations provide a Dirac equation for the nucleon and Klein-Gordon equations for the boson fields. The static solution is obtained by solving the stationary Dirac equation

$$\{-i\boldsymbol{\alpha}\cdot\nabla+\beta M^*(\mathbf{r})+V(\mathbf{r})\}\psi_i(\mathbf{r})=\varepsilon_i\psi_i(\mathbf{r}) . \quad (4)$$

The effective mass $M^*(\mathbf{r})$ is no longer a constant and is written in terms of $\sigma(\mathbf{r})$ as

$$M^*(\mathbf{r})=M+g_\sigma\sigma(\mathbf{r}) . \quad (5)$$

The potential $V(\mathbf{r})$ contains only a timelike component

$$V(\mathbf{r})=g_\omega\omega^0(\mathbf{r})+g_\rho\tau^3\rho^0(\mathbf{r})+e\frac{1-\tau_3}{2}A^0(\mathbf{r}) . \quad (6)$$

The spatial currents vanish due to the requirement of spherical symmetry. Charge conservation guarantees that only the third isotopic component of $\boldsymbol{\rho}$ survives. Using the eigenfunctions $\psi_i(\mathbf{r})$ obtained by solving the eigenvalue equation (4), the fourth component of the vector currents and the scalar density are written as

$$\rho_s(r)=\sum_{i=1}^{A}\bar{\psi}_i(r)\psi_i(r) ,$$
$$\rho_v(r)=\sum_{i=1}^{A}\bar{\psi}_i(r)\gamma^0\psi_i(r) , \quad (7)$$
$$\rho_3(r)=\sum_{i=1}^{A}\bar{\psi}_i(r)\tau_3\gamma^0\psi_i(r) ,$$
$$\rho_p(r)=\sum_{i=1}^{A}\bar{\psi}_i(r)\frac{1-\tau_3}{2}\gamma^0\psi_i(r) .$$

The Klein-Gordon equations are

$$(-\Delta+m_\sigma^2)\sigma(r)=-g_\sigma\rho_s(r)-g_3\sigma^2(r)-g_4\sigma^3(r) ,$$
$$(-\Delta+m_\omega^2)\omega^0(r)=g_\omega\rho_v(r) , \quad (8)$$
$$(-\Delta+m_\rho^2)\rho^0(r)=g_\rho\rho_3(r) ,$$
$$-\Delta A^0(r)=e\rho_p(r) .$$

These equations have to be solved iteratively. The total energy is calculated as

$$E=\int d^3rH(r) ,$$

with

$$H(r)=\sum_i\psi_i^\dagger[-i\nabla\cdot\boldsymbol{\alpha}+\beta M^*(r)+V(r)]\psi_i$$
$$+\tfrac{1}{2}(\nabla\sigma)^2+U(\sigma)$$
$$-\tfrac{1}{2}\{(\nabla\omega^0)^2+m_\omega^2\omega^{0^2}+(\nabla\rho^0)^2+m_\rho^2\rho^{0^2}+(\nabla A^0)^2\} . \quad (9)$$

We subtract from the energy a center-of-mass correction, $E_{\text{c.m.}}=\frac{3}{4}41A^{-1/3}$ MeV [12]. Hence, we do not consider a possible isotopic effect on $E_{\text{c.m.}}$, which needs a systematic study.

Other quantities can be calculated from the wave functions ψ_i, where the single-particle states are specified by κjm in the usual notation. The ground states are assumed to have nucleons filling all levels up to the Fermi levels for neutrons and protons. The occupation probability of each state in a partially occupied single-particle level is taken as $n_j/(2j+1)$, with n_j the number of particles in the level and $2j+1$ its degeneracy. This prescription corresponds to the BCS description with zero gap energy. We may try the BCS description assuming a fixed pairing strength, which is the subject of our future study together with the consideration of possible deformation effect.

We shall describe here how the parameters of the relativistic Hartree theory, m_σ, m_ω, m_ρ, g_σ, g_ω, and g_ρ, are determined in each set discussed in this paper. The principle of determining these parameters is as follows. The nuclear matter saturation values, $(E/A)_{\text{sat}}$ and ρ_{sat}, are used to fix the ratio g_σ/m_σ and g_ω/m_ω. The symmetry energy is used to determine g_ρ/m_ρ. Using the experimentally known masses for m_ω and m_ρ, g_ω and g_ρ are then fixed. The sigma meson mass is unknown. Hence, one fixes the mass m_σ using the properties of finite nuclei [10]. Their binding energies and radii are very sensitive to m_σ, as will be discussed in Sec. III. The parameters for the nonlinear potential $U(\sigma)$, g_3 and g_4, are adjusted to provide the best results for the properties of finite nuclei. The parameter sets NL1 and NL2 are obtained by a least-squares fit to the masses and radii of stable nuclei [11]. We provide a list in Table I of the parameter sets, denoted by HS, L1, TS, NL1, and NL2, that are used in the present study.

III. NUMERICAL RESULTS

We show in Fig. 1 the dependence on m_σ of the binding energy B/A and the root-mean-square charge radius R_c for ^{16}O for the parameter sets in which the σ potential is linear. The results indicate that these quantities are extremely dependent on the value of m_σ. As m_σ increases, B/A also increases while R_c decreases, resulting in a scalar potential which becomes narrower and deeper. The experimental values are indicated by the arrows. Horowitz and Serot have chosen m_σ so as to reproduce the charge radius [10]. This procedure provides $m_\sigma=520$ MeV as indicated in Fig. 1. As clearly seen, this choice gives a binding energy smaller than the experimental one. Toki *et al.* have chosen $m_\sigma=597.6$ MeV so as to reproduce B/A [13], which is also indicated in Fig. 1. We note that this choice yields smaller nuclear radii. We conclude that the linear parameter sets cannot reproduce both the binding energy and the nuclear size.

The ρ-meson strength is fixed by the symmetry energy. The symmetry energy a_{sym} has been determined by Myers and Swiatecki [16] in the liquid drop model. Using their value, $a_{\text{sym}}=28.1$ MeV, one obtains $g_\rho=2.78$ [13]. A

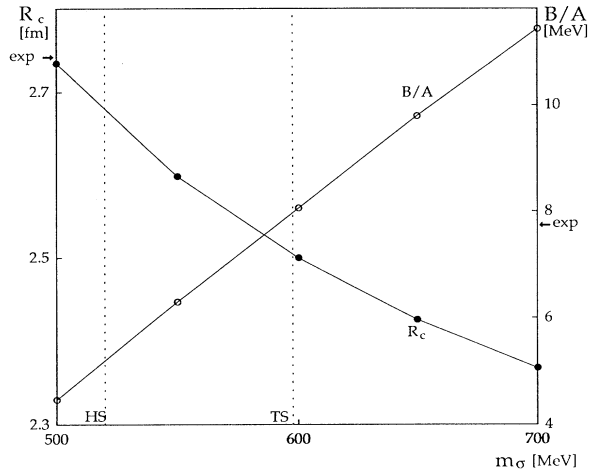

FIG. 1. The binding energy per particle B/A and the charge radius R_c of ^{16}O as a function of the sigma meson mass m_σ. Experimental values are indicated by arrows. The choices of HS and TS are depicted by dashed lines with HS and TS beside each line, respectively.

larger value $a_{\text{sym}}=35$ MeV has been obtained by using the droplet model with shell corrections [17], giving $g_\rho=4.04$. This value is used in the set HS [10]. Reinhard *et al.* [11] have made a least-squares fit of all the parameters of the Lagrangian to the binding energies and the radii of selected stable nuclei. They found $g_\rho=5.507$, which provides a much larger $a_{\text{sym}}=43.9$ MeV for NL2, and $g_\rho=4.975$ with $a_{\text{sym}}=43.5$ MeV for NL1.

The parameter sets used in this study, HS, TS, L1, NL1, and LN2, are listed in Table I. As we have discussed, HS and TS differ in that m_σ was chosen to reproduce the mean charge radius in HS, whereas in TS, it was chosen to reproduce the binding energy. Note that the values of g_ρ in HS and TS are thus slightly different. The parameter sets NL1 and NL2 contain nonlinear terms for the sigma meson field that are determined by fitting the parameters to the binding energies and nuclear radii of stable nuclei [11]. We also study the parameter set L1, which does not include an isovector term, as an example in which the symmetry energy is small. The effective mass and the incompressibility of symmetric nuclear matter, M^*/M and K, are also listed for each set in Table I. The effective mass is about 0.55–0.65 and the incompressibility is about 550–600 MeV for the linear σ parametrizations. For the nonlinear ones, it is considerably reduced to about 400 MeV for NL2, and about 200 MeV for NL1. Note that the symmetry energy attains its minimum value, $a_{\text{sym}}=21.7$ MeV, for the set L1 and its maximumvalue of 43.9 MeV for the set NL2.

Due to the spherical model we use, we limit our study to even-even nuclei and choose proton magic nuclei, O, Ca, Ni, Zr, Sn, and Pb, for the calculations. As an example, we show in Table II the numerical results for the various nuclear radii and the binding energy per particle for the Ca isotopes. We define the proton and neutron drip lines in terms of the most neutron-deficient and the most neutron-rich nuclei, respectively. These, in turn, are determined by the nuclei unstable to proton or neutron emission, which, in our calculations, will be those with two neutrons less than the most neutron-deficient ones or with two neutrons more than the most neutron-rich ones, respectively.

TABLE I. The parameter sets used in the present study, HS [10], TS [13], L1 [12], NL1 [11], and NL2 [11]. M, m_σ, m_ω, and m_ρ are the masses of the nucleon and the sigma, omega, and rho mesons. g_σ, g_ω, and g_ρ are the coupling strengths of the sigma, omega, and rho mesons with the nucleon. g_3 and g_4 are the nonlinear coupling strengths of the sigma meson. M^*, K, and a_{sym} are the relativistic Hartree values for the nucleon effective mass, incompressibility, and symmetry energy at the saturation point of symmetric nuclear matter.

	HS	TS	L1	NL1	NL2
M (MeV)	939.0	939.0	938.0	938.0	938.0
m_σ (MeV)	520.0	597.6	550.0	492.25	504.89
m_ω (MeV)	783.0	783.0	783.0	795.359	780.0
m_ρ (MeV)	770.0	770.0		763.0	763.0
g_σ	10.47	11.206	10.30	10.138	9.111
g_ω	13.80	12.72	12.60	13.285	11.493
g_ρ	4.04	2.78		4.975	5.507
g_3 (fm^{-1})				−12.172	−2.304
g_4				−36.265	13.783
M^*/M	0.541	0.548	0.53	0.57	0.67
K (MeV)	545.0	547.2	626.3	211.7	399.2
a_{sym} (MeV)	35.0	28.1	21.7	43.5	43.9

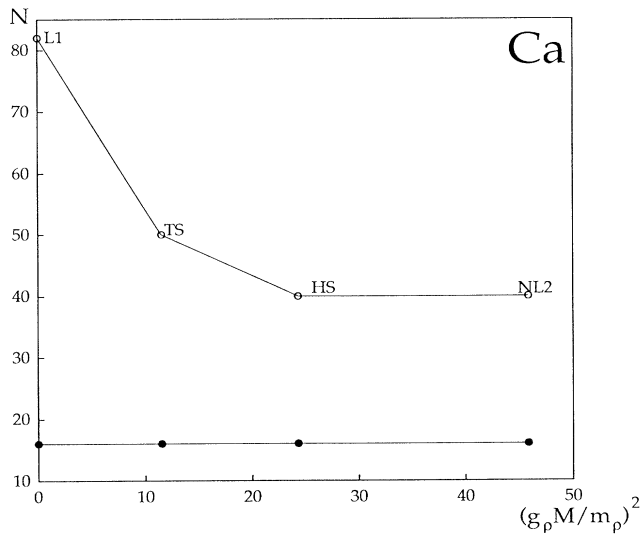

FIG. 2. The neutron numbers at the neutron (open circle) and the proton (closed circle) drip lines for Ca isotopes as a function of the rho meson strength g_ρ. These numbers are calculated with the parameter sets indicated as L1, TS, HS, and NL2 beside each circle, which have the corresponding rho meson strength.

We first discuss the parameter sets in which the σ potential is linear. For the binding energy, the TS values are close to the NL1 and NL2 results, while the HS values are much smaller. On the other hand, for the nuclear radii, the HS values are close to the NL1 and NL2 results, while the TS values are much smaller. Hence, the sets with linear σ potentials show the same discrepancies far from the stability line that they show for stable nuclei.

It is interesting to note that, while the proton drip line is insensitive to differences in the parameter sets, the neutron drip line changes greatly from set to set. Although not shown in Table II, the neutron drip line extends to a large difference in neutron and proton number for the set L1, where the symmetry energy is minimum. This feature is seen in Fig. 2, where the proton and the neutron drip lines for the Ca isotopes are plotted against the rho meson strength g_ρ. The neutron number of the nucleus at the neutron drip line decreases from $N=82$ to $N=40$ as a function of g_ρ. In addition, it is interesting to note that the "last" neutron number for each parameter set is $N=82$ for L1, $N=50$ for TS, and $N=40$ for HS and NL2, which are all magic numbers. On the other hand, the neutron number at the proton drip line is unchanged and is $N=16$ for all cases except NL1. Similar observations can be made for the other elements.

We find that the calculated results with NL1 and NL2 compare extremely well with experiment. We show in Fig. 3 the neutron number dependence of the binding energies per particle B/A for NL1 and NL2. It is amazing to see how well the NL1 results agree with experiment. The NL2 results are less satisfactory. The isovector strength g_ρ of NL2 seems too strong. We comment here, however, that the NL1 results become unstable for light neutron deficient nuclei, such as ^{14}O and ^{36}Ca, for a reason different from the usual one of negative separation energy. This is a well-known result and is due to the wrong sign of g_4, which causes nuclear matter with a density slightly higher than the normal one to be unstable [9]. This is the reason why we cannot apply the parameter set NL1 for the discussion of nuclear matter. We believe, however, that the results obtained with NL1 for nuclei with stable solutions are reliable, since NL1 seems to generate the nuclear matter properties around the normal matter density such as the saturation property and the incompressibility.

The good agreement with experimental data makes us confident in using our calculations to predict the proton and neutron radii of unstable nuclei, shown in Fig. 4. The results with NL1 and NL2 are almost identical. The neutron radii are found to become much larger than pro-

TABLE II. The proton, neutron, and charge radii, R_p, R_n, and R_c, and the binding energy per particle B/A for Ca isotopes between the proton and the neutron drip lines obtained using four of the parameter sets.

Nuclei	Param.	R_p (fm)	R_n (fm)	R_c (fm)	B/A (MeV)	Nuclei	Param.	R_p (fm)	R_n (fm)	R_c (fm)	B/A (MeV)
^{36}Ca	HS	3.396	3.158	3.491	−5.78	^{38}Ca	HS	3.386	3.254	3.482	−6.14
	TS	3.132	2.945	3.235	−7.33		TS	3.133	3.027	3.236	−7.68
	NL1						NL1	3.393	3.260	3.488	−8.20
	NL2	3.367	3.153	3.463	−7.57		NL2	3.352	3.235	3.499	−8.12
^{40}Ca	HS	3.387	3.332	3.483	−6.51	^{42}Ca	HS	3.379	3.410	3.474	−6.58
	TS	3.145	3.091	3.247	−8.08		TS	3.142	3.158	3.245	−8.15
	NL1	3.407	3.360	3.502	−8.56		NL1	3.401	3.477	3.496	−8.56
	NL2	3.349	3.309	3.446	−8.60		NL2	3.352	3.399	3.448	−8.58
^{44}Ca	HS	3.375	3.477	3.470	−6.66	^{46}Ca	HS	3.374	3.535	3.470	−6.76
	TS	3.143	3.215	3.246	−8.27		TS	3.146	3.265	3.249	−8.42
	NL1	3.398	3.522	3.493	−8.57		NL1	3.397	3.359	3.492	−8.58
	NL2	3.358	3.481	3.454	−8.56		NL2	3.368	3.555	3.464	−8.54
^{48}Ca	HS	3.375	3.588	3.471	−6.86	^{50}Ca	HS	3.394	3.733	3.490	−6.72
	TS	3.152	3.309	3.254	−8.60		TS	3.171	3.487	3.273	−8.32
	NL1	3.398	3.648	3.493	−8.60		NL1	3.411	3.769	3.506	−8.47
	NL2	3.380	3.625	3.476	−8.50		NL2	3.399	3.765	3.494	−8.30
^{52}Ca	HS	3.414	3.854	3.508	−6.61	^{54}Ca	HS	3.440	3.929	3.534	−6.42
	TS	3.194	3.607	3.295	−8.10		TS	3.225	3.651	3.326	−7.88
	NL1	3.420	3.867	3.514	−8.36		NL1	3.467	3.974	3.560	−8.15
	NL2	3.416	3.894	3.511	−8.10		NL2	3.444	3.962	3.538	−7.90
^{56}Ca	HS	3.467	3.993	3.560	−6.25	^{58}Ca	HS	3.495	4.048	3.588	−6.13
	TS	3.259	3.690	3.358	−7.72		TS	3.292	3.725	3.391	−7.62
	NL1	3.514	4.067	3.606	−7.96		NL1	3.560	4.150	3.651	−7.81
	NL2	3.472	4.027	3.565	−7.72		NL2	3.501	4.088	3.593	−7.56
^{60}Ca	HS	3.514	4.144	3.606	−6.05	^{62}Ca	HS				
	TS	3.316	3.822	3.413	−7.47		TS	3.332	3.851	3.429	−7.28
	NL1	3.580	4.247	3.671	−7.71		NL1				
	NL2	3.518	4.196	3.610	−7.40		NL2				
^{64}Ca	TS	3.348	3.878	3.445	−7.12	^{66}Ca	TS	3.365	3.904	3.461	−6.98
^{68}Ca	TS	3.381	3.929	3.477	−6.88	^{70}Ca	TS	3.398	3.953	3.493	−6.81

ton radii as the nuclei become distant from the stability line. Both NL1 and NL2 provide very good results for stable nuclei, whose values are known experimentally. Using the set NL1, we find for the neutron radii of stable nuclei, $R_n = 3.65$ fm (^{48}Ca) 4.34 fm (^{90}Zr), and 5.79 fm (^{208}Pb), as compared to the proton radii, $R_p = 3.40$ fm (^{48}Ca), 4.20 fm (^{90}Zr), and 5.47 fm (^{208}Pb) with similar values for NL2. Although most microscopic models provide differences between the proton and neutron radii similar to the present ones, these large differences contradict the common notion that such differences are less than 0.1 fm for stable nuclei [18,19]. We note that the difference between proton and neutron radii does not depend very much on the rho meson coupling strength and hence the asymmetry energy as discussed already in Toki *et al.* [13].

Another interesting feature seen in Fig. 4 is the smooth increase of the radius R_n with the neutron number N. The proton radius R_p also increases with N, but cannot follow the increase of R_n. We usually find that R_n increases more rapidly than the systematics as the neutron drip line is approached. Though slight, R_p shows a similar tendency to increase suddenly near the neutron drip line. It would be interesting to obtain more experimental information on the radii of unstable nuclei.

As an example, we show in Figs. 5 and 6 the proton and neutron density distributions of the Zr isotopes calculated with the NL2 set. We see a gradual change of the

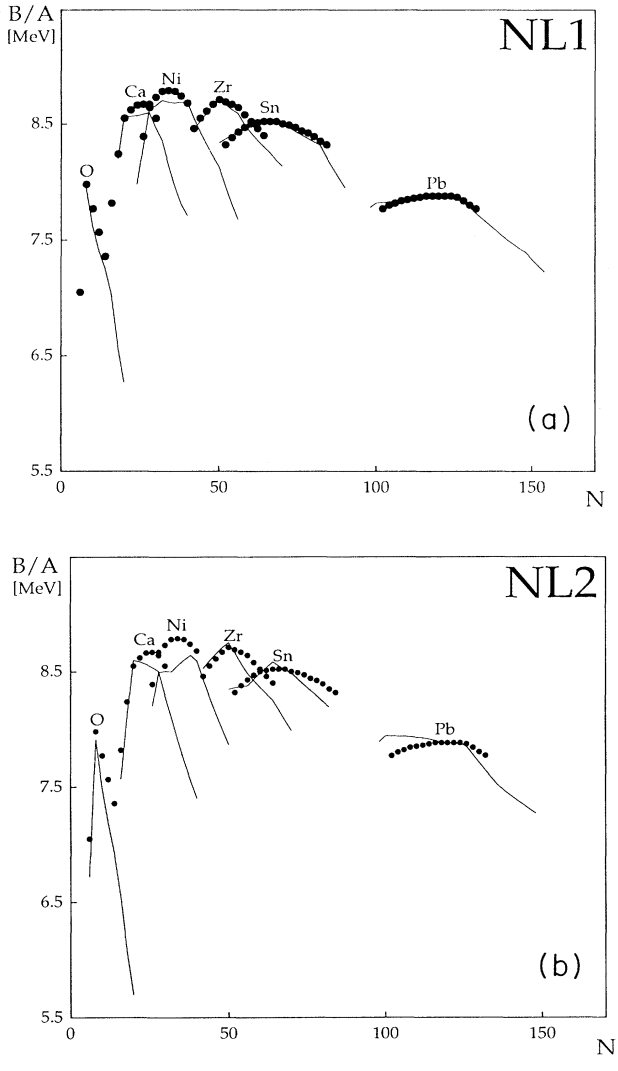

FIG. 3. Binding energy per particle B/A for O, Ca, Ni, Zr, Sn, and Pb isotopes as a function of the neutron number calculated with the parameter sets (a) NL1 and (b) NL2. Experimental values are shown by closed circles.

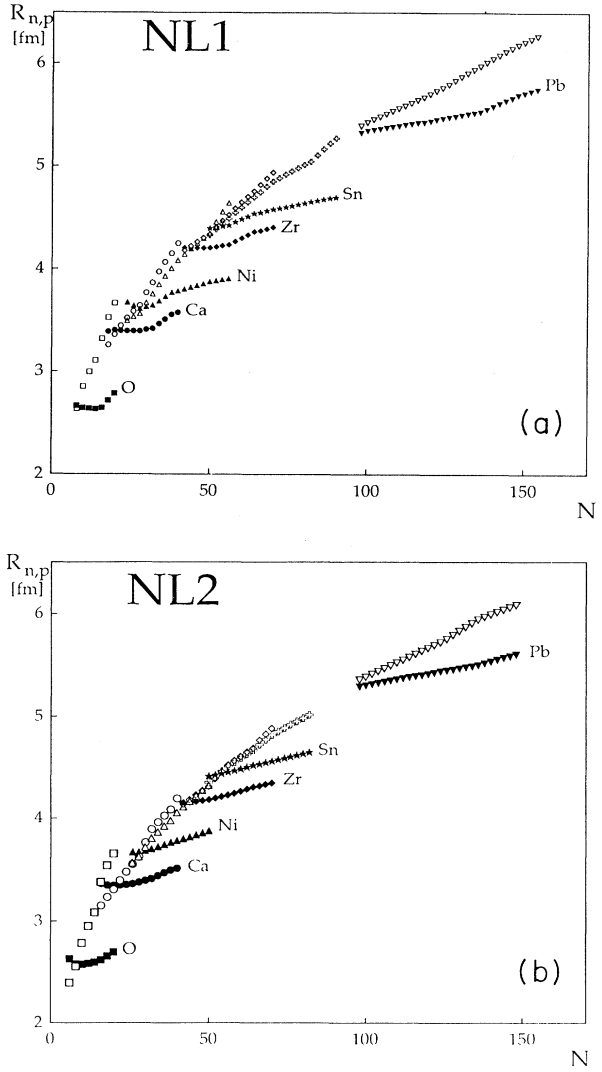

FIG. 4. Proton and neutron root-mean-square radii R_p and R_n for O, Ca, Ni, Sn, Zr, and Pb isotopes as a function of the neutron number calculated with the parameter sets (a) NL1 and (b) NL2.

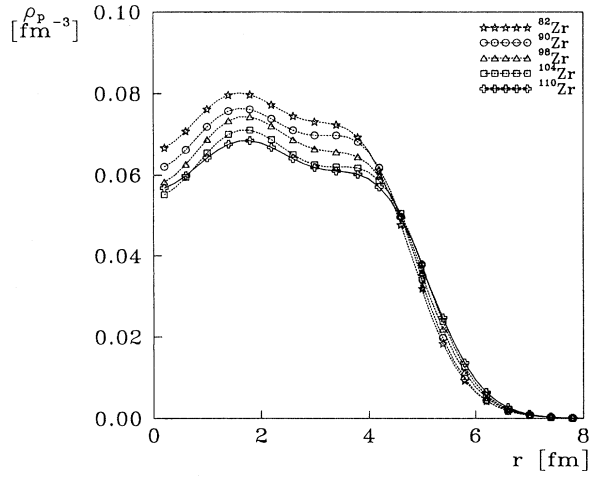

FIG. 5. Proton density distributions for various Zr isotopes as a function of the radial coordinate r calculated with the set NL2.

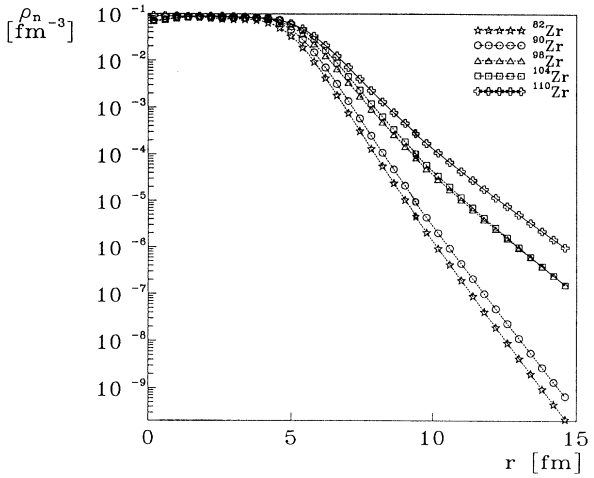

FIG. 7. Neutron density distributions for various Zr isotopes on a logarithmic scale as a function of the radial coordinate r calculated with the set NL2.

density distributions with the neutron number. We also show in Fig. 7 the neutron density distributions of the Zr isotopes on a logarithmic scale so that their asymptotic behavior can be better seen. The tails of the neutron distributions extend further as the nuclei approach the neutron drip line. The central part of the proton distribution decreases with N while its radius increases so as to keep the proton number fixed. The central part of the neutron distribution increases only slightly, whereas its radius increase greatly with N. In the logarithmic plot, we clearly see the tails of the neutron distributions. At the neutron drip line, the neutron binding energy becomes small and the neutron distribution extends to large distances.

We show in Fig. 8 the neutron and the proton drip lines in the Z-N plane for NL1 and NL2. Both parameter sets provide similar lines. The area between the drip lines is much smaller than the generally accepted one, which is obtained using the mass formula [20]. The area depends strongly on the symmetry energy and the latter attain their largest values, $a_{\rm sym} \sim 45$ MeV, for the sets NL1 and NL2. This result, together with the large difference between the proton and neutron radii, will have a large effect on the r-process of nucleosynthesis.

An interesting problem we would like to address here is the magic number of nuclei far from the stability line. Since the magic numbers are a consequence of the central and spin-orbit potentials, it could happen that the num-

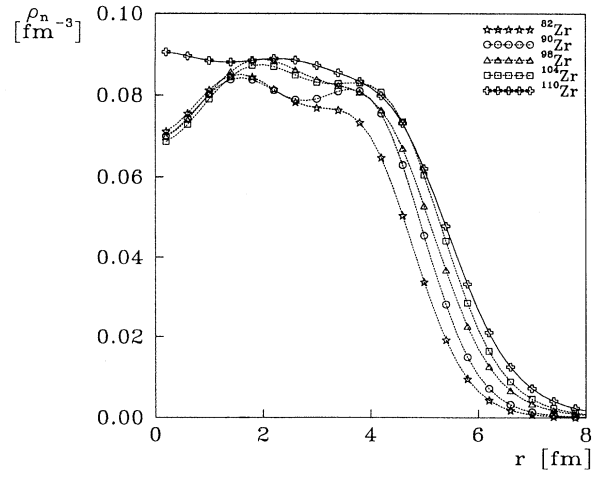

FIG. 6. Neutron density distributions for various Zr isotopes as a function of the radial coordinate r calculated with the set NL2.

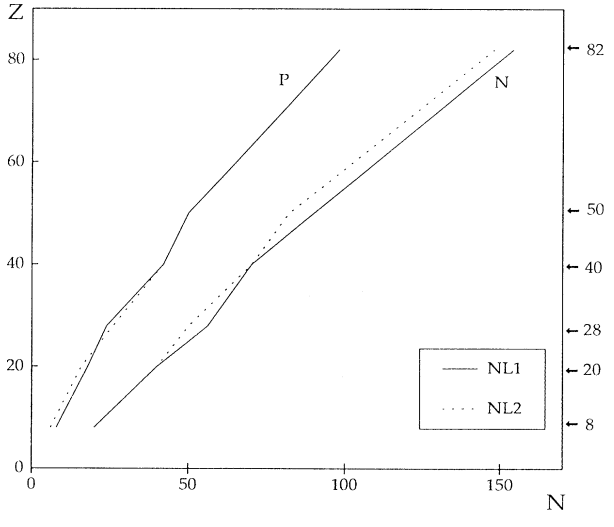

FIG. 8. The proton and neutron drip lines calculated with the sets NL1 (solid line) and NL2 (dashed line) in the Z-N plane. The numbers shown on the right-hand side of the figure are the proton numbers of the magic proton nuclei that are calculated.

bers change with distance from the line. In particular, the sequence of magic numbers at $N=20$, 28, 40, 50 etc., due to the lowering of the energies of high-spin single-particle levels of higher principal shells, could be modified. We want to study this problem in the present framework, since the central potential and the spin-orbit interaction are completely correlated in the relativistic theory. There is some experimental evidence of a change in magic number at $N=20$ for $Z\sim 11$ [21], which was called an "island of inversion" [22]. Hence, we want to study the single-particle spectra around $N=20$.

We plot in Figs. 9 and 10 the single-particle spectra for protons and neutrons of nuclei with $N=20$ and Z ranging from 10 to 26, obtained by using the set NL2. In general, as Z increases, the single-particle energies for protons go up in energy, while those for neutrons come down. This behavior is caused by the isovector interaction, i.e., the rho meson. The energy gap at $N=20$, which is the separation between the $f_{7/2}$ and $s_{1/2}$ or $d_{3/2}$ levels, does not become smaller when Z is very different from N. This finding completely agrees with those of Warburton *et al.* [23] and of Campi *et al.* [24], obtained in shell-model and nonrelativistic Hartree-Fock calculations, respectively. We can conclude that the magic number at $N=20$ does not disappear within the present framework. The "disappearance of the magic number" at $N=20$, instead, seems to be caused by the onset of deformation. Since both protons and neutrons are at the beginning of a major shell, the addition of neutrons in the f shell favors prolate deformation which is further favored by the promotion of protons to the same shell. We also note that the pairing correlations for nucleons in high-j shells are quite large and act to decrease the magic number effect [23].

We would now like to discuss the role of the rho meson, which becomes progressively more important for $N\gg Z$. For this purpose, we show in Fig. 11(a) the scalar, vector, and isovector-vector potentials for $Z=12$ and $N=20$ for the NL2 set. Reflecting the large difference between the proton and the neutron distribution, the isovector-vector potential $g_\rho\rho^0$ behaves as expected. Its magnitude is, however, much smaller than that of the other potentials even though the g_ρ of NL2 is larger than that of the other parameter sets. Although it is small, the isovector part contributes appreciably to the central potential, since the latter is only weakly negative due to

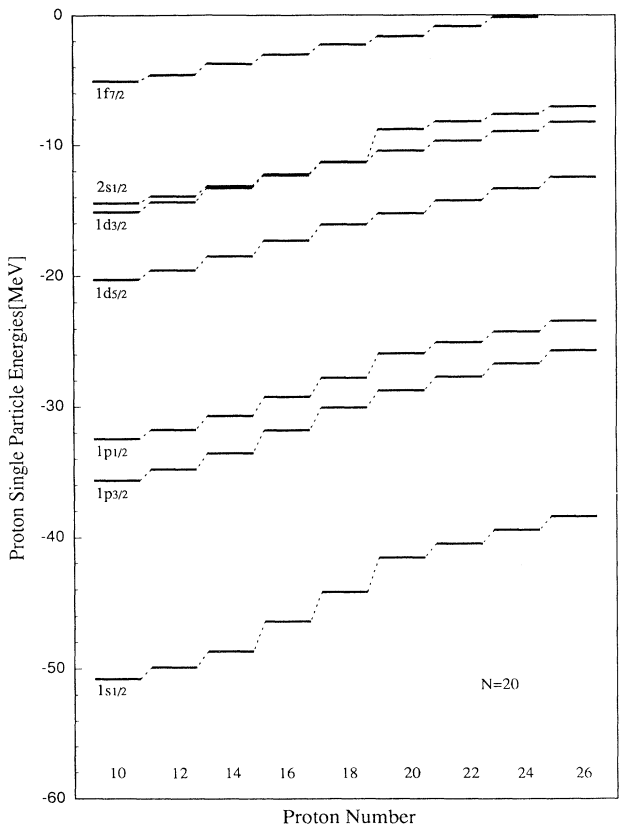

FIG. 9. Proton single-particle spectra of $N=20$ isotones between the neutron and the proton drip lines as a function of the proton number Z calculated with the set NL2.

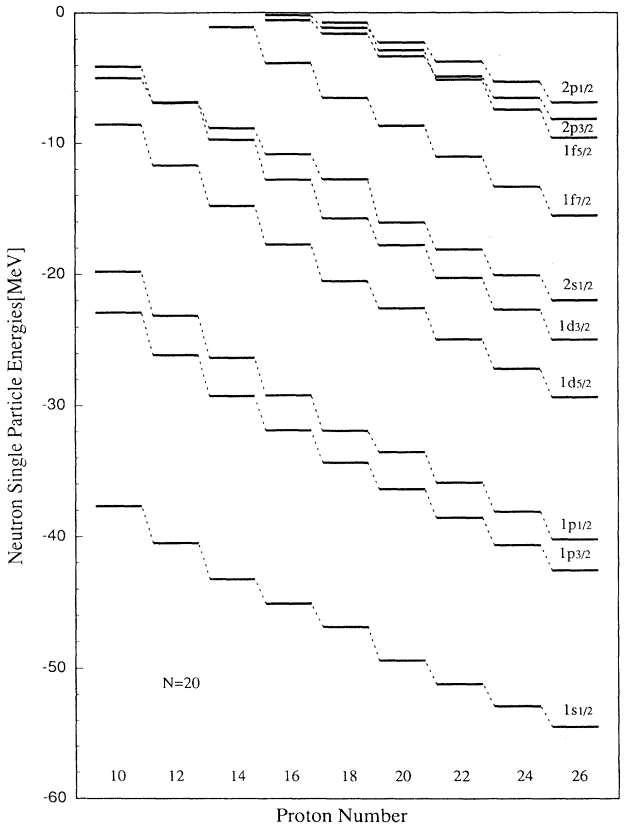

FIG. 10. Neutron single-particle spectra of $N=20$ isotones between the neutron and the proton drip lines as a function of the proton number Z calculated with the set NL2.

cancellation between the strongly attractive $g_\sigma\sigma$ and the strongly repulsive $g_\omega\omega^0$. The net potentials for protons and for neutrons are depicted in Fig. 11(b). The large difference between the potentials for protons and neutrons makes their single-particle energies quite different. However, the isovector contribution to the spin-orbit potential is negligibly small since the isoscalar fields σ and ω^0 add to provide an extremely large spin-orbit potential. This is the reason the magic numbers are not influenced, even when the proton number differs greatly from the neutron number and the isovector term contributes its most.

IV. CONCLUSIONS

We have studied the properties of nuclei far from the stability line in the relativistic Hartree theory. As examples, we have chosen the isotopes of the proton magic even-even nuclei O, Ca, Ni, Zr, Sn, and Pb and five parameter sets, HS, L1, TS, NL1, and NL2. The choice of set NL2 in addition to NL1 is due to its positive g_4, which permits its application to nuclear matter. We have found that the neutron drip line depends strongly on the symmetry energy, while the proton drip line is rather insensitive to the parameter sets. The neutron radii become much larger than the proton ones as the difference between the neutron number N and the proton number Z becomes large. This should have a large effect on neutron capture rates and beta-decay strengths for nuclei far from the stability line. The spherical relativistic Hartree theory does not change the magic numbers. Instead, the disappearance of the magic number at $N=20$ with $Z\sim 11$ would seem to be caused by deformation. We plan to study this in more detail in the near future.

The nonlinear σ potential terms are necessary to provide a good account of both the binding energies and the nuclear radii [12]. The present study has shown that the set NL1, determined by a least-squares fit to the experimental data for stable nuclei, provides the best results for nuclei far from the stability line. The set NL2, determined in the same manner, yields slightly less satisfactory results. The ρ meson strength, which becomes progressively more important as N deviates from Z, seems to be too large in the set NL2. This statement is based on the comparison with experimental binding energies shown in Fig. 3 [25]. It would be very interesting to see if a readjustment of the ρ meson strength would improve the agreement with the binding energies of unstable nuclei without losing the quality of fit obtained for stable nuclei. The known proton drip line is already consistent with the calculations made using the set NL2 [26].

It is extremely important to continue to study nuclei off the stability line, both experimentally and theoretically, before reaching definite conclusions on nuclear properties far from the stability line. It would be very useful to make RBHF calculations [14], although they are extremely time consuming, for a few typical nuclei to check the predictions of the relativistic Hartree theory. In this respect, the RBHF results for nuclear matter properties are extremely encouraging. Analyzing the vector-type potential of the RBHF results as a function of the matter density, we clearly see the necessity of also introducing nonlinear terms for vector potential (ω and/or ρ). The introduction of such a nonlinear potentials may remove the difficulty of the negative g_4 encountered in the set NL1. A search for a better parameter set is in progress.

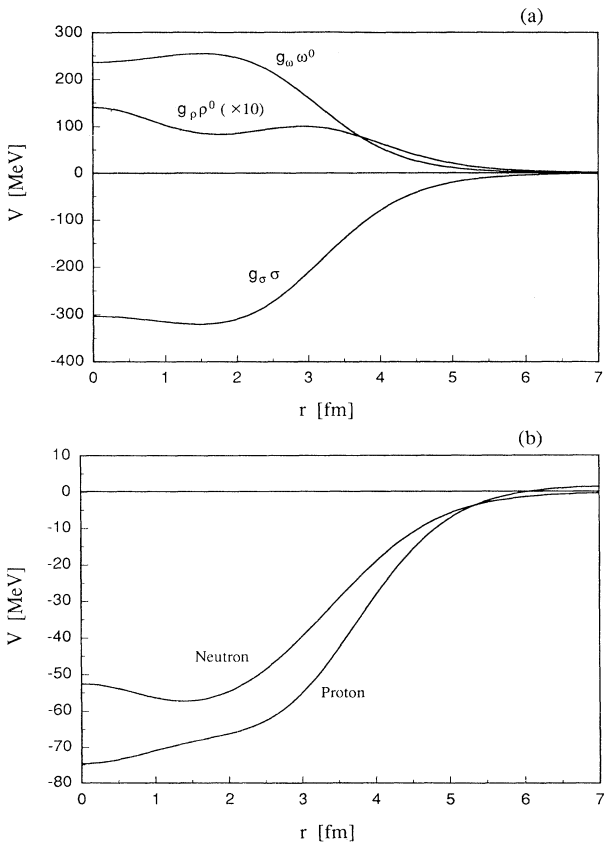

FIG. 11. (a) Relativistic Hartree potentials $g_\sigma\sigma$, $g_\omega\omega^0$, and $g_\rho\rho^0$ as a function of the radial coordinate r calculated for the nucleus with $Z=12$ and $N=20$ with the set NL2. (b) The central potentials for protons and neutrons obtained from the relativistic Hartree potentials as a function of the radial coordinate r calculated with the set NL2.

ACKNOWLEDGMENTS

We acknowledge useful discussions with Y. Sugahara on various aspects of infinite matter. We are grateful to R. Brockmann for fruitful discussions on the RBHF theory and thank C. Horowitz for providing us his relativistic Hartree code, TIMORA. B.V.C. acknowledges the support of the CNPq–Brazil and D.H. the support provided by the exchange program between the CNPq–Brazil and the Ministry of Education of Japan.

[1] I. Tanihata, T. Kobayashi, S. Shimoura, K. Sugimoto, and T. Minamisono, Proceedings of the First International Conference on Radioactive Nuclear Beams, Berkeley, 1989 (unpublished), p. 429, and references therein.
[2] I. Tanihata, H. Hamagaki, O. Hashimoto, Y. Shida, N. Yoshikawa, K. Sugimoto, O. Yamakawa, T. Kobayashi, and N. Takahashi, Phys. Rev. Lett. **55**, 2676 (1985).
[3] I. Tanihata, Proceedings of the Symposium in Honor of A. Arima held at Santa Fe in 1990 (unpublished).
[4] P. A. Seeger, D. D. Clayton, and W. Fowler, Astrophys. J. Suppl. **11**, 121 (1965).
[5] T. Kajino, G. J. Mathews, and G. M. Fuller, Astrophys. J. **364**, 7 (1990).
[6] R. I. Epstein, S. A. Colgate, and W. C. Haxton, Phys. Rev. Lett. **61**, 2038 (1988).
[7] J. R. Walecka, Ann. Phys. **83**, 491 (1974).
[8] B. D. Serot and J. D. Walecka, Adv. Nucl. Phys. **16**, 1 (1986).
[9] P. G. Reinhard, Rep. Prog. Phys. **52**, 439 (1989).
[10] C. J. Horowitz and B. D. Serot, Nucl. Phys. **A368**, 503 (1981).
[11] P. G. Reinhard, M. Rufa, J. Maruhn, W. Greiner, and J. Friedrich, Z. Phys. A **323**, 13 (1986).
[12] Y. K. Gambhir, P. Ring, and A. Thimet, Ann. Phys. **198**, 132 (1990).
[13] H. Toki, Y. Sugahara, D. Hirata, I. Tanihata, and B. Carlson, Nucl. Phys. **A524**, 633 (1991).
[14] R. Brockmann and R. Machleidt, Phys. Rev. C **42**, 1965 (1990).
[15] A. Hosaka, K. Kubo, and H. Toki, Nucl. Phys. **A444**, 76 (1985).
[16] W. D. Myers and W. J. Swiatecki, Nucl. Phys. **81**, 1 (1966).
[17] P. A. Seeger and W. M. Howard, Nucl. Phys. **A238**, 491 (1975).
[18] R. H. Basel and C. Wilkin, Phys. Rev. **174**, 1179 (1968).
[19] A. Chaumenaux, V. Layly, and R. Shaeffer, Ann. Phys. **116**, 247 (1978).
[20] W. D. Meyer and W. J. Swiatecki, Ann. Phys. **55**, 395 (1969).
[21] C. Thibault, R. Klapisch, C. Rigaud, A. M. Poskanzer, R. Prieels, L. Lessard, and W. Reisdorf, Phys. Rev. C **12**, 644 (1975).
[22] B. H. Wildenthal and W. Chung, Phys. Rev. C **22**, 2260 (1980).
[23] E. K. Warburton, J. A. Becker, and B. A. Brown, Phys. Rev. C **41**, 1147 (1990).
[24] X. Campi, H. Flocard, A. K. Kerman, and S. Koonin, Nucl. Phys. **A251**, 193 (1975).
[25] A. H. Wapstra and G. Audi, Nucl. Phys. **A432**, 55 (1985).
[26] C. Detraz, Proceedings of the International Conference on Nuclear Physics, Brazil, 1989 (unpublished), p. 337.